

LECTURES ON TIDES

UNIS, Longyearbyen, 23 - 27 Sept. 2013

by

B. Gjevik

Department of Mathematics, University of Oslo

P.O.Box 1053 Blindern, Oslo, Norway

email: bjorng@math.uio.no

Contents

1	Introduction	3
2	Tide generating force	5
3	Harmonic decomposition of the tide generating force	11
4	Ocean response	12
5	Harmonic constants and tidal predictions	12
6	Harmonic analysis of tidal records	16
7	Laplace's tidal equation	18
8	Free wave solution to LTE. Kelvin waves.	19
9	Numerical models	22
10	Tidal charts for the Barents Sea	22
11	Tidal currents	28
12	Drift and dispersion of particles in the tidal flow	29
13	Mean sea level (MSL)	31
14	Exercises	33

1 Introduction

The periodic rise and fall of the sea surface has fascinated man from the earliest ages. Obviously people must early have noticed the connection between high and low water and the position of the Moon and the Sun. Due to the regularity of the phenomena it became closely associated with the flow of time as the very name tides indicates.

When Newton (1697) first formulated the theory of gravitation he also discovered the nature of the tide generating force. Newton's equilibrium theory of tides explained the observed dominant semidiurnal periodicity of ocean tides. Up to then it had been a mystery that high water occurs both with Moon overhead and also about 12 hours later when the Moon is on the other side of the earth. Today Newton's equilibrium theory (see section 2) provides the correct tide generating force to which the oceans respond hydrodynamically in a rather complicated fashion. Although Newton discovered the true astronomic nature of the tide, it was Laplace (1775) who derived the first hydrodynamic equations of ocean tides. Laplace's tidal equations contain the tide generating force in terms of Newton's equilibrium tide as the forcing function.



Figure 1: The Moon is barren and lifeless, but its gravitational force induces strong tidal currents in the world's oceans and thereby affects life on the Earth. Here the Moon is photographed in perigee position when it is closest to the Earth.

Due to the complexity of Laplace's tidal equations little progress was made in solving these equations with realistic bottom topography and coastlines before powerful

Periodic cycles of the Moon

There are four important cycles of the Moon with periods 27–29 days.

Nr.	Type	Period (mean solar day)
1	Recurrence of Moon's phase (synodic Moon).	29.5306
2	Oscillation in Moon's distance. from Earth (anomalistic Moon).	27.5546
3	Oscillation in the Moon's declination.	27.2122
4	Time of one orbit around the ecliptic relativ to the vernal equinox (sidereal Moon).	27.3216

If two periodic events (signals), recurring with period T_1 and T_2 respectively, are in phase at time $t = 0$ they will be in phase again after $t = T_n = nT_1$ where the integer number n is determined from $nT_1 = (n + 1)T_2$. This leads to $n = T_2/(T_1 - T_2)$ and $T_n = T_1T_2/(T_1 - T_2)$ ($T_1 > T_2$). With $T_1 = 29,5306$ days and $T_2 = 27,5546$ days we find that it will be $T_n = 1.13$ year between the recurrence of perigee at either full or new Moon. Similarly it will take 8.9 years between each time perigee coincides with the vernal equinox.

computers became available. Since then Laplace's equations have been the basis of most modern tidal modelling.

The observation and mathematical treatments of tides were greatly advanced by Lord Kelvin (Thomson, 1868) who introduced the method of *harmonic analysis* of tides. Both the astronomical forcing and the responding ocean tide are represented as a series of harmonic tidal components each with its characteristic frequency, determined from the regular almost periodic motion of the Moon and the Sun. With this representation the time dependent ocean tides, can be accurately described when a few time independent harmonic constants in terms of amplitude and phases are known. The harmonic constants are characteristic for every geographical point in the ocean and along the coasts. These constants may be determined by harmonic analysis of observed time series of sea level changes, with regular and sufficient frequent time sampling, or by solving the Laplace's tidal equations with realistic bottom topography and coastline configurations.

The tides particularly in coastal waters appear as a markedly dominant part of the ocean current variability. Since sea level changes and shifting currents associated with the tides are of great importance for all maritime activity, coastal engineering and management there is an enormous number of scientific publications devoted to the subject. The reviews by Cartwright (1977), Schwiderski (1980, 1986), and Davies et al. (1996) survey central parts of the literature. It is impossible to cover this vast subject within the frame of this short lecture series. We will therefore restrict to discuss in some detail, three important aspect, the nature of the *tide generating force*, *harmonic analysis* of tide and some aspects of *tidal modelling*. The presentation and examples in this lecture series rely heavily on my own and my co-workers research on tides and may for this reason be somewhat biased with respect to citations and references.

2 Tide generating force

The tide generating force is due to the gravitation of the Moon and the Sun. In order to see this we shall consider a system of two spherical globes, the Earth and the Moon, with masses m_e and m_l respectively. From the center of the Earth, O , to a point P on the surface of the Earth we draw a distance vector \vec{r} and the corresponding distance vectors from O and P to the Moon (M) are denoted \vec{R} and \vec{d} respectively (fig. 2). The length of these vectors are written $r = |\vec{r}|$, $R = |\vec{R}|$ and $d = |\vec{d}|$. Since d and R are large compared to the radius of the Moon it can be regarded as a point, M , and we obviously have

$$\vec{r} + \vec{d} = \vec{R} \quad (1)$$

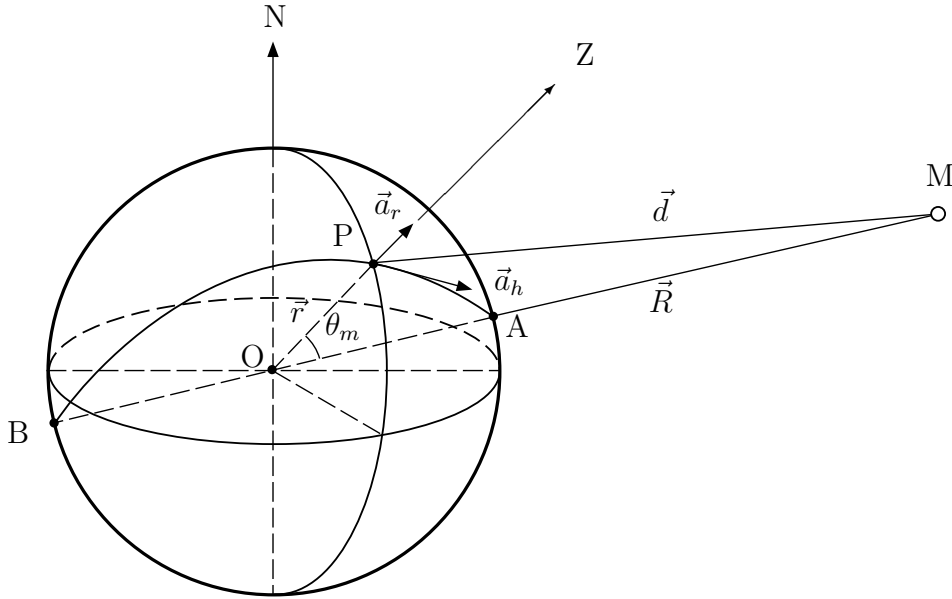


Figure 2: The system Earth-Moon. N and Z denote North and the Zenit direction respectively.

From the law of gravitation (Newton 1697), the gravitational force on the Earth is

$$G \frac{m_e m_l}{R^2} \frac{\vec{R}}{R} \quad (2)$$

where G is the gravitation constant. This force gives the center of the Earth an acceleration.

$$\vec{a}_0 = G \frac{m_l}{R^2} \frac{\vec{R}}{R}$$

If we disregard the rotation of the Earth and consider the Earth to be rigid and undeformable every point on the Earth will experience the same acceleration. The acceleration at the point P due to the direct gravitational pull of the Moon is

$$\vec{a}_p = G \frac{m_l}{d^2} \frac{\vec{d}}{d}$$

The difference between \vec{a}_p and \vec{a}_0 is the tidal acceleration

$$\vec{a} = \vec{a}_p - \vec{a}_0 = G m_l \left[\frac{\vec{d}}{d^3} - \frac{\vec{R}}{R^3} \right] \quad (3)$$

which corresponds to a tidal force pr unit mass. The vector \vec{a} is obviously contained in the plane through O, P and M .

From the trigonometric cosines relation for the triangle OPM

$$d^2 = R^2 + r^2 - 2Rr \cos \theta_m$$

where angle θ_m is the angular zenith distance of the Moon. Hence

$$d = R \sqrt{1 - 2 \frac{r}{R} \cos \theta_m + \frac{r^2}{R^2}}$$

By expanding the square root in a series after the small parameter $\frac{r}{R}$ and neglecting terms of order $(\frac{r}{R})^2$.

$$d \cong R \left[1 - \frac{r}{R} \cos \theta_m \right] + O \left(\frac{r}{R} \right)^2$$

Again by series expansion

$$\frac{1}{d^3} = \frac{1}{R^3 (1 - \frac{r}{R} \cos \theta_m)^3} \cong \frac{(1 + 3 \frac{r}{R} \cos \theta_m)}{R^3}$$

By using the latter relation together with eq. (1), the tidal acceleration, eq. (3), can be written:

$$\vec{a} = \frac{Gm_l r}{R^3} \left[3 \frac{\vec{R}}{R} \cos \theta_m - \frac{\vec{r}}{r} \right] \quad (4)$$

When introducing the acceleration of gravity at the Earth's surface

$$g = \frac{Gm_e}{r^2}$$

the expression (4) can be written

$$\vec{a} = g \frac{m_l}{m_e} \left(\frac{r}{R} \right)^3 \left[3 \frac{\vec{R}}{R} \cos \theta_m - \frac{\vec{r}}{r} \right] \quad (5)$$

which shows that the tidal acceleration is a very small fraction of g . With parameters for the Earth–Moon system, $\frac{m_l}{m_e} = 0.012$, $\frac{r}{R} = 0.017$ the fraction is of the order 10^{-7} .

Equation (5) shows that \vec{a} is a sum of a vertical vector always pointing downward along the vertical and a vector in the direction \vec{R} i. e. towards the Moon for $\theta_m < \frac{\pi}{2}$ and opposite \vec{R} when $\frac{\pi}{2} < \theta_m < \pi$. Hence there will be a component of the acceleration directed either towards the point A under the Moon or towards the antipodal point B on the other side of the Earth (fig. 3).

The vector \vec{a} can be decomposed in a vertical component, a_r , and a horizontal component, a_h . The latter being directed along the great circle arch APB (fig.2). Since $\vec{R} \cdot \vec{r} = Rr \cos \theta_m$ we have

$$a_r = \vec{a} \cdot \frac{\vec{r}}{r} = g \frac{m_l}{m_e} \left(\frac{r}{R} \right)^3 [3 \cos^2 \theta_m - 1] \quad (6)$$

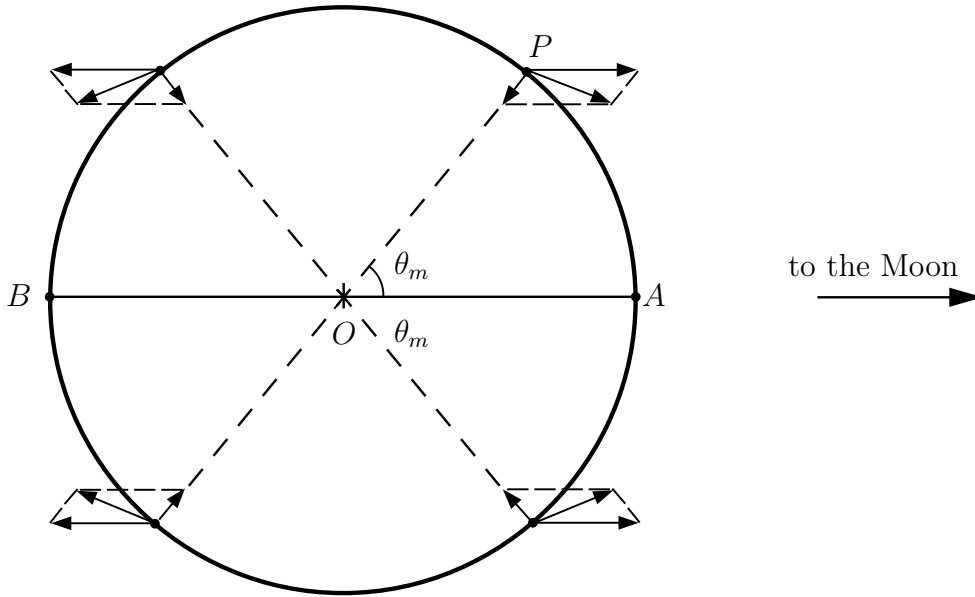


Figure 3: The direction of the tidal acceleration.

and since $|\vec{R} \times \vec{r}| = Rr \sin \theta_m$

$$a_h = \left| \vec{a} \times \frac{\vec{r}}{r} \right| = \frac{3}{2} g \frac{m_l}{m_e} \left(\frac{r}{R} \right)^3 \sin 2\theta_m \quad (7)$$

Here we can introduce the Moon's horizontal parallax π_m defined by

$$\sin \pi_m = \frac{r}{R}$$

which is a commonly used parameter for the position of the Moon.

Imaging now that the Earth is covered by a thin sheet of water subject to the tide generating force of the Moon. In order to be in equilibrium the surface of the water will deform in order to set up an adverse pressure gradient counteracting the horizontal tidal force. The equilibrium condition is

$$-g \frac{\partial \tilde{\eta}_m}{r \partial \theta_m} - \frac{3}{2} g \frac{m_l}{m_e} \sin^3 \pi_m \sin 2\theta_m = 0$$

where $\tilde{\eta}_m$ is the vertical displacement of the water. By integration we obtain

$$\tilde{\eta}_m = \frac{3}{4} \frac{m_l}{m_e} r \sin^3 \pi_m \cos 2\theta_m + C$$

where C is a constant of integration which is determined by the requirement that there is no change in water volume by the deformation. This leads to $C = \frac{1}{3}$ and

$$\tilde{\eta}_m = \frac{1}{4} \frac{m_l}{m_e} r \sin^3 \pi_m (3 \cos 2\theta_m + 1) \quad (8)$$

This expression shows that there will be high water under the Moon at A and also the point B on the opposite side of the Earth. A zone of low water extends around the globe with lowest water level for $\theta_m = \frac{\pi}{2}$ as sketched in figure 5.

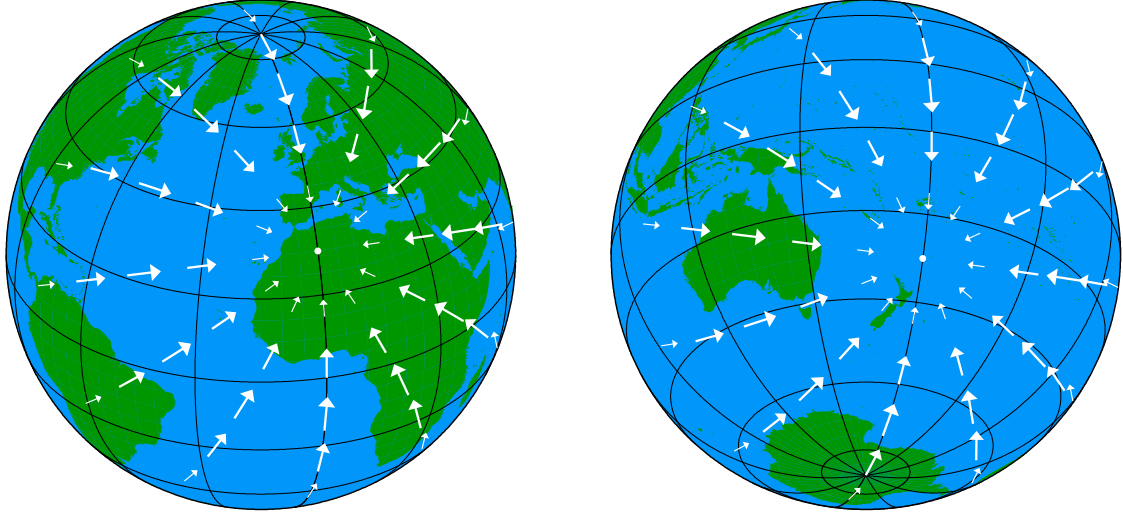


Figure 4: The horizontal component of the tidal force is directed toward a point right under the Moon and the image on the opposite side of the Earth. Here the Moon stands over North Africa and the image is located north of New Zeland in the Pacific Ocean. The same force field will appear if the Moon was located above the image point. As the Earth rotates the field will move westward.

With the Moon moving in the equatorial plane there will, for each location on the Earth, be high water when the Moon passes the meridian and another equally high water about 12.4 hours later when the Moon is on the opposite side of the Earth. Hence, the expression (8) explains nicely the semi-diurnal variation of sea level. When the Moon has a northern or southern declination there will be an asymmetry between two consecutive high waters. Therefore equation (8) also explains the diurnal equality i.e. the difference in sea level rise between two consecutive high water. The surface displacement given by eq. (8) is called the *equilibrium tide* and in absence of continent it is thought to follow the Moon when the Earth rotates. It corresponds to the idealized situation where the water masses adjust instantaneous to the motion of the Moon and the rotation of the Earth.

Table 1 Astronomical constants.

Mass of the Earth:	m_e	$5.974 \cdot 10^{24}$	kg
Mass of the Sun:	m_s	$1.991 \cdot 10^{30}$	kg
Mass of the Moon:	m_l	$7.347 \cdot 10^{22}$	kg
Mean distance Earth-Moon	R	$3.844 \cdot 10^5$	km
Mean distance Earth-Sun	R	$1.496 \cdot 10^8$	km
Radius of the Earth	r	$6.370 \cdot 10^3$	km

The equilibrium tide is often used as a potential for the tide generating force. The strength of the horizontal component of the tidal acceleration (7) and the equilibrium tide (8) will vary with the position of the Moon and its distance from the Earth. Maximum tidal acceleration will occur when the Moon is closest to the Earth (perigee)

and minimum acceleration when the Moon is in apogean position. The variation the acceleration from minimum to maximum is about 20% of the mean value.

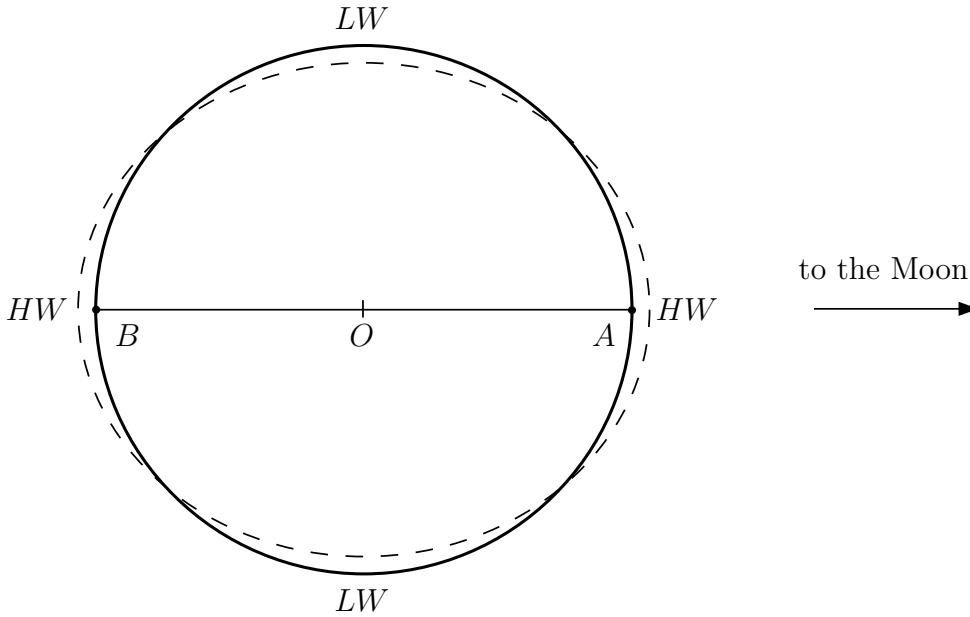


Figure 5: The equilibrium tide. HW : high water, LW : low water.

Here we have only established, to lowest order of accuracy, the expression for the equilibrium tide due to the action of the Moon. A similar expression will clearly also appear from the action of the Sun

$$\tilde{\eta}_s = \frac{1}{4} \frac{m_s}{m_e} r \sin^3 \pi_s (3 \cos 2\theta_s + 1)$$

where m_s and π_s denote the mass and the horizontal parallax of the Sun respectively, and θ_s is zenith distance of the Sun. Although the mass of the Sun is much larger than the mass of the Moon the parallax for the Sun is much less than the parallax of the Moon. The equilibrium tide due to the Sun is therefore about half of the Moon's. The combined effect of the Moon and the Sun leads to an expression for the total equilibrium tide

$$\tilde{\eta} = \tilde{\eta}_m + \tilde{\eta}_s \quad (9)$$

With the astronomical constants in table 1 we find the maximum values of the equilibrium tide $\tilde{\eta}_m = 0.35$ m and $|\tilde{\eta}_s| = 0.15$ m. Hence the maximum amplitude of the combined equilibrium tide from the Moon and the Sun will be 0.50 m. This is considerably less than the ocean tide in most places and we will later, in section 4, see how the equilibrium tide is amplified in the ocean. Since the position of the Moon and the Sun can be calculated with a high degree of accuracy the parallax and zenith distances is known as highly accurate functions of time. Hence we can calculate the spatial and temporal variation of the equilibrium tide or equivalently the tide generating force.

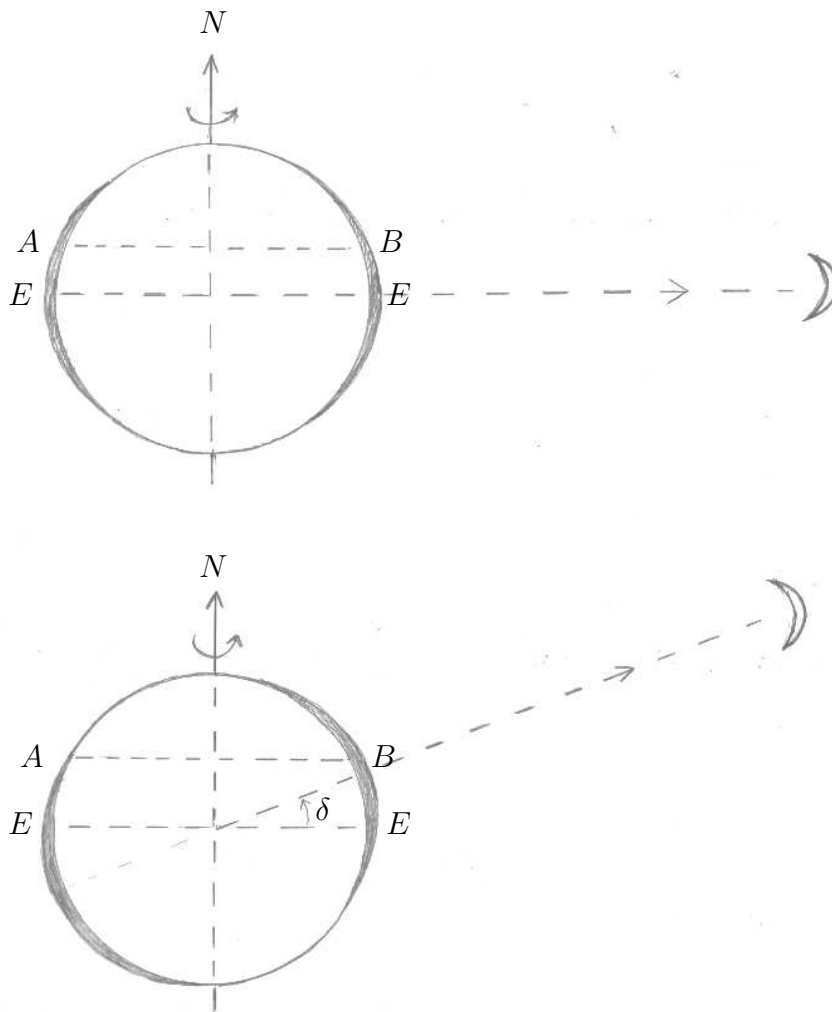


Figure 6: Schematic illustration of the effect of the Moon's declination on the equilibrium tide.. With the Moon in the equator plane (declination $\delta = 0$) the tides at A and B have the same height (upper figure). With the Moon above the equator plane (declination $\delta > 0$) the tides at A is lower than the tide at B (lower figure).

3 Harmonic decomposition of the tide generating force

The tide generating force, or equivalently the equilibrium tide, can be decomposed into a series of *harmonic components* or partial tides. Each component or *constituent* has a amplitude determined from the equilibrium tide and a period corresponding to periods for the orbital motion of the Moon, Earth and the Sun. The major constituents have either period around 12 hours or 24 hours and are therefore classified as *semi-diurnal* or *diurnal species* respectively. It has been shown that at a point with geographical coordinates θ, φ , the equilibrium tide can be written as sum of cosines function.

$$\tilde{\eta} = \sum_i \tilde{\eta}_i(\theta) \cos(\omega_i t + \chi_i + \nu_i \varphi) \quad (10)$$

where $\tilde{\eta}$ is the *amplitude*, ω_i is the *frequency*, χ_i is an *astronomical argument* and ν_i an index equal 1 for diurnal components and 2 for semi-diurnal. The geographical coordinates are here colatitude θ and longitude φ

The astronomical argument can be expressed in terms of mean longitude of the Sun, Moon and lunar perigee usually relative to Greenwich midnight . Formulas for calculating the astronomical arguments are given for example by Schwiderski (1980, 1986).

The average time lapse from one transit of the Moon over the Greenwich meridan to the next is $2 \cdot 12.42 = 24.82$ hours. The astronomical argument of M_2 , i.e. χ_{M_2} measured in degrees, will give the time of transit of the Moon: $t_G = (24.82 \times \chi_{M_2})/360$. If the astronomical argument is zero it means that the Moon transits the meridian at midnight (in GMT time) on that particular day.

Six of the major astronomical tidal components are listed in table 1 with their symbol, period, and frequency. Here the component M_2 represents the tidal force of an imaginary Moon circulating around the Earth in the equator plane with the mean speed of the real Moon. Similarly the component S_2 corresponds to a Sun circulating in the equator plane. The effect of the declination changes are accounted for by the diurnal component K_1 and the ellipticity of the Moon's orbit by the component N_2 . Similar, albeit a less intuitive, interpretation can be given to the other astronomical components.

Table 2 List of major tidal harmonic components.

<i>Symbol</i>	<i>Period (T)</i> <i>hours</i>	Frequency (ω) 10^{-4} rad/s	<i>Description</i>
M_2	12.42	1.40519	principal lunar, semidiurnal
S_2	12.00	1.45444	principal solar, semidiurnal
N_2	12.66	1.37880	elliptical lunar, semidiurnal
K_2	11.97	1.45842	declinational luni-solar, semidiurnal
K_1	23.93	0.72921	declinational luni-solar, diurnal
O_1	25.82	0.67598	principal lunar, diurnal
S_a	year		meteorological, annual

4 Ocean response

The ocean response is basically a linear process which means that the sea level changes at a given location can be expressed as a corresponding sum of harmonic components with the same prevailing frequencies as appeared in the decomposition of the equilibrium tide eq. (10). This is a common property of all linear harmonic oscillators, a well-known process also from other branches of physics. Hence sea level at a location with colatitude θ and east longitude φ can be written

$$\eta(\theta, \varphi, t) = \sum_i H_i(\theta, \varphi) \cos[\omega_i t + \chi_i - \delta_i(\theta, \varphi)] \quad (11)$$

The amplitude $H_i(\theta, \varphi)$ and Greenwich phase $\delta_i(\theta, \varphi)$ are usually referred to as the *harmonic constants* for the component i and t is Greenwich (GMT) time or Universal time (UT). The amplitude and the phase for each component depend in a very complicated way on the dynamical properties of the ocean basin i.e. depth, shape, size, dissipation as well as the amplitude and phase of the corresponding partial equilibrium tide. If for example one of the forcing frequency in the sum (10) happens to coincide with an eigen frequency of the basin oscillations large amplitude tides may occur.

Amplification of the tide may also occur when the ocean tide propagates over the shelf into shallow water, and when irregularities in the coastal topography act as obstacles to the tide. As we already have seen it follows from eq. 9 that the amplitude of the equilibrium tide is of order 0.5 m. Since in many places the sea level changes of the tides are several meters it is clear that significant amplification occurs in many ocean basins. We shall discuss the variation of tidal amplitudes and phases on basin scale in section 10.

5 Harmonic constants and tidal predictions

The harmonic constants for each tidal constituent at a certain location can be determined by harmonic analysis of observed time series of surface elevation from that particular location (see section 6) or by numerical tidal models for the surrounding basin (see section 9). As an example we shall consider the tides at Longyearbyen.

Table 3 Harmonic constants for sea level at Longyearbyen.

Component	$H_i(cm)$	$\delta_i(deg)$
M_2	52.2	356.0
S_2	19.9	40.0
N_2	10.0	329.6
K_2	5.7	38.0
K_1	10.2	221.0
O_1	3.1	77.0

From long series of records of sea level the harmonic constants at Longyearbyen are determined by Polarinstituttet, Tromsø, Norway and published annually in the official tables of tides from Norges Sjøkartverk (2013).

An interpretation to the phase angle δ_{M_2} for M_2 can be given as follows: Consider for simplicity a day when the Moon transit the Greenwich meridan at midnight (GMT time) i.e. $\chi_{M_2} = 0$. Then the first high water after the lunar transit will occur when the argument of the cosine function $(\omega_{M_2}t - \delta_{M_2}) = 0$. Hence the time delay is $t_d = \delta_{M_2}/\omega_{M_2}$. Since the phase angle usually is measured in degrees it is more convenient to write

$$t_d = T_{M_2} \frac{\delta_{M_2}}{360}$$

where $T_{M_2} = 12.42$ hours is the period of the M_2 component. This leads to $t_d = 12.28$ hours delay of high water. Now it is also high water 12.42 hours before. This means that it is also high water about 8 minutes before the transit of the Moon in Greenwich.

With this set of constants in table 3 it is easy to demonstrate the characteristics of tidal oscillations at Longyearbyen (figure 8). The calculations are done for September 2013 on basis of eq. 11. The astronomical arguments, χ_i , for the various components are determined by a separate program which calculates the position of the Moon and the Sun (Schwiderski, 1986). Figure 8 shows clearly the significance of the various components. With M_2 only (a), the sea level varies regularly as a harmonic oscillation with amplitude 52.2 cm and period 12.42 hours. With S_2 added (b), the beat cycle of the *spring* and the *neap* tides appears. Here the highest spring tides occur around the 8th and 21th of September about 2 days after new and full Moon respectively, with neap tides around the 14th and 29th of September. The delay of the spring tide relative to the time for new and full Moon, here about 2 days, is called *the age of the tide* which is influenced in a complicated way by the dissipation of tidal energy in the basin. An estimate of the age of the tide (in hours) can be calculated from the formula

$$0.984 \cdot (\delta_{S_2} - \delta_{M_2})$$

where δ_{S_2} and δ_{M_2} are the phase angles measured in degrees for the S_2 and M_2 components respectively. With values from table 3, $\delta_{S_2} = 360+40$ and $\delta_{M_2} = 356$, the average age of the tide in Longyearbyen is found to be 43.3 hours. The amplitude of the neap tide is 32.3 cm, i.e. the difference between the amplitude of the M_2 and the S_2 constituents, while the amplitude of the spring tide is 72.1 cm i.e. the sum of the amplitudes of M_2 and S_2 .

With N_2 added to S_2 and M_2 (c), an asymmetry between the first and the second neap tides appears. The neap tide around 14th of September is considerably larger than the neap tide around 29th of September. This is due to the variation of the distance between the Moon and the Earth. In September 2013 the minimum distance of 367 387 km (perigee) occurs on the 15th and maximum distance 404 308 km (apogee) on the 27th. The variation in the distance to the Moon introduces a difference in height of the two neap tides. Finally (d) where the diurnal component K_1 is added clearly shows the *diurnal inequality* with a noticeable difference in amplitude for two consecutive high or low waters. How the variation of the declination of the Moon produces a diurnal inequality is shown schematically in fig. 6.

The tides at Longyearbyen is dominated by the semi-diurnal constituents M_2 and S_2 which lead to the characteristic neap-spring cycles. A similar tidal structure is common all over the Norwegian and the Barents Seas. In some other oceans, for example on the Pacific coast of USA, the diurnal component is large, leading to a more complex tidal structure (mixed tide).

With the same technique as described above the sea level changes at Longyearbyen are calculated for a period in January 1993 and compared with available observations (figure 9). We see that the predictions are in very good agreement with the observations, but there is some systematic differences for example from the 3th to the 5th day.

During this period the observations are generally lower than the predictions an effect most likely due to the influence of atmospheric forces i.e. wind stress and pressure. Tidal predictions for harbours along the coast of Norway and Svalbard are available in ref. [24]. The website from the Norwegian Hydrographic Service, Statens Kartverk: <http://vannstand.no/> also provides sea level observations.



Figure 7: The tidal wave propagates from the open ocean into Isfjorden and Adventfjorden (picture). Short records of sea level oscillations are available from temporarily operating tidal stations at Hotellneset and Longyearbyen harbour. A permanent tidal station is operated at Ny-Alesund by Statens Kartverk which measures the sea level variations relative to the ground. At this station the vertical and horizontal motion of the ground are also monitored with accurate GPS and VLBI techniques in order to determine land upheaval and absolute sea level changes (Sato et al. 2006). Data from the station in Ny-Alesund is available on <http://www.vannstand.no>. Picture from franziundmagieinspitzbergen.blogspot.com

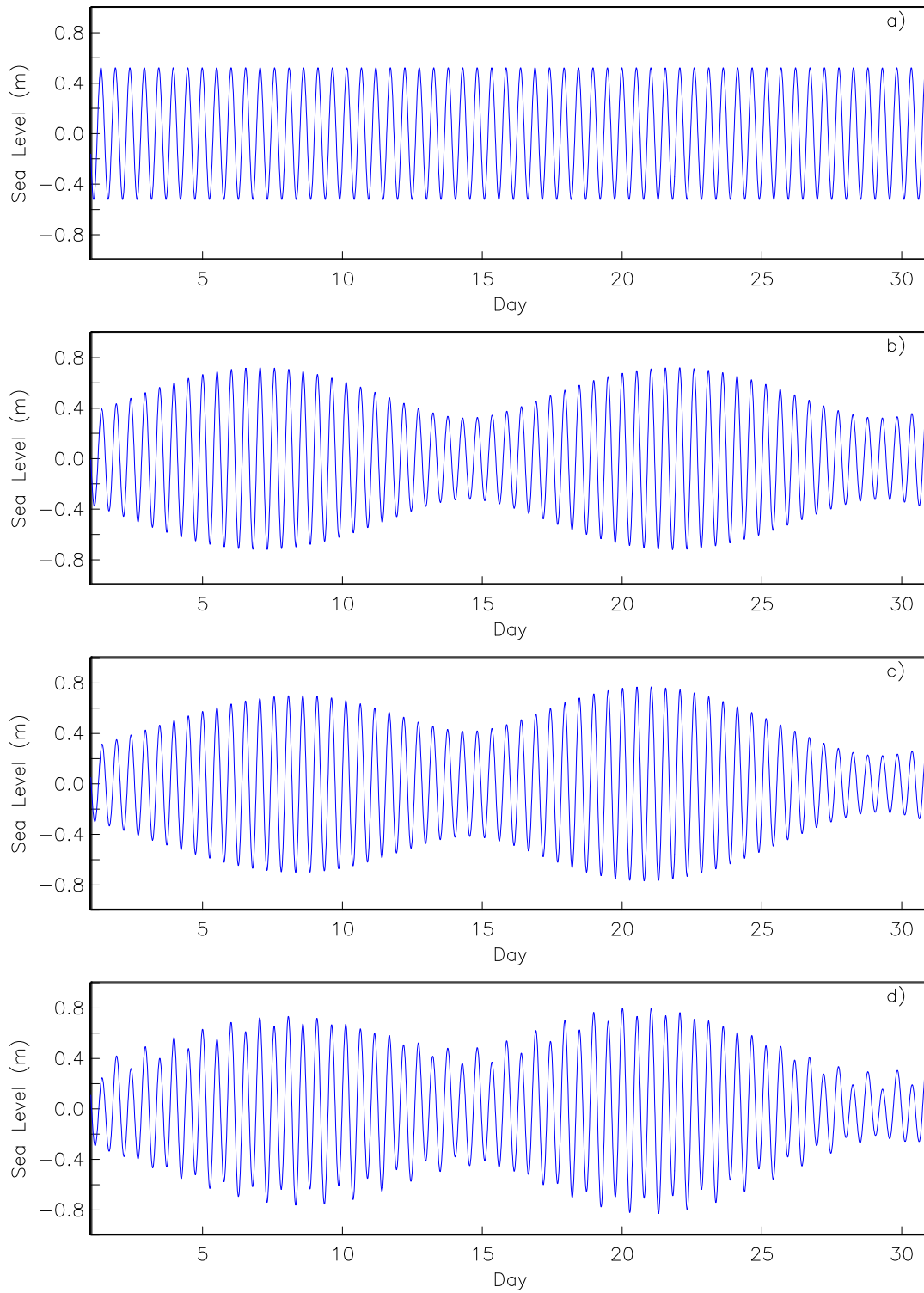


Figure 8: Tides at Longyearbyen 1-30 September 2013. a) Only M_2 , b) M_2+S_2 , c) $M_2+S_2+N_2$, d) $M_2+S_2+N_2+K_1$. New Moon 5 Sept. and full Moon 19 Sept. Lunar perigee 15 Sept. and apogee 27 Sept. Day starts at midnight UT (GMT).

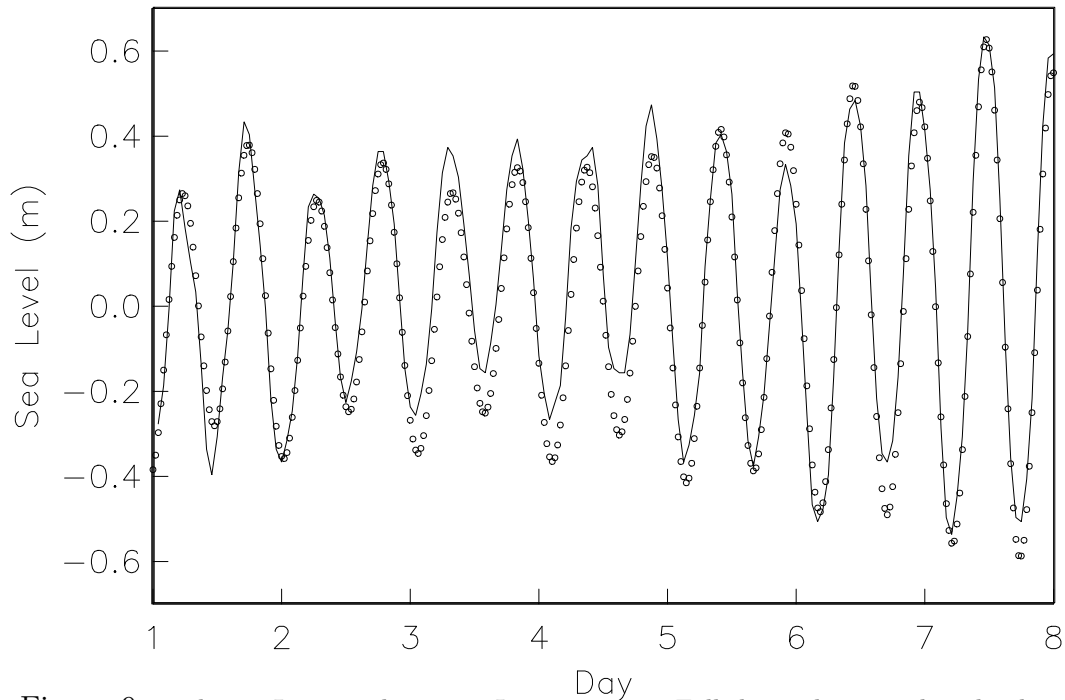


Figure 9: Tides at Longyearbyen 1-8 January 1993. Full drawn line; predicted tide with the six components listed in table 2. Circles; observations with 1 hour sampling interval. Observational data from Mr. T. Eiken, Polarinstittet, Oslo.

6 Harmonic analysis of tidal records

In order to provide an understanding of the basic principles of harmonic analysis we shall here give a simplified description of the method. The method as it is formulated here is closely related to the method of least square error, frequently used in statistics and analysis of measurement errors in experimental physics. Assume that at a station the height of sea level, h , relative a fixed point has been recorded at regular time intervals Δt over a time span $0 < t < t_m$

$$h = \{h_k\}, \quad k = 1, 2, 3, \dots k_{\max}$$

where $t_m = (k_{\max} - 1)\Delta t$. For tidal records the sampling interval, Δt , normally is from 10 minutes to 1 hour. The mean height of sea level is

$$\bar{h} = \frac{1}{k_{\max}} \sum_1^{k_{\max}} h_k \quad (12)$$

and the displacement of the sea level relative to the mean value

$$\eta = \{\eta_k\} = \{h_k - \bar{h}\}, \quad k = 1, 2, 3 \dots k_{\max}$$

We may for simplicity assume that the sampling is sufficient dense so that we may regard η as a continuous function of time

$$\eta = \eta(t) \quad (13)$$

We shall now, again for simplicity, assume that the variation of η with time is dominated by one distinct tidal frequency with period T_i and that the length of the record is long enough to contain several oscillations, i.e. $t_m > T_i$. Let try to approximate the function $\eta(t)$ by a harmonic component

$$\eta_s(t) = H_i \cos(\omega_i t - \kappa_i)$$

where κ_i contain both the astronomical argument and the phase of the component as defined in eq. 11. This expression can be rewritten in the form

$$\eta_s(t) = A_i \cos \omega_i t + B_i \sin \omega_i t$$

where $A_i = H_i \cos \kappa_i$ and $B_i = H_i \sin \kappa_i$. The integrated square difference between $\eta(t)$ and $\eta_s(t)$ is

$$I = \int_0^{t_m} [\eta(t) - \eta_s(t)]^2 dt$$

Now the difference, I , is a function of A_i and B_i and we may determine these coefficients so that I attains a minimum value. The conditions for this is obviously.

$$\frac{\partial I}{\partial A_i} = 0; \quad \frac{\partial I}{\partial B_i} = 0$$

which leads to

$$\int_0^{t_m} [\eta(t) - \eta_s(t)] \cos \omega_i t dt = 0$$

$$\int_0^{t_m} [\eta(t) - \eta_s(t)] \sin \omega_i t dt = 0$$

By substituting for $\eta_s(t)$ in the integrals we find after rearrangements

$$\int_0^{t_m} \eta(t) \cos \omega_i t dt - A_i \int_0^{t_m} \cos^2 \omega_i t dt - B_i \int_0^{t_m} \cos \omega_i t \sin \omega_i t dt = 0$$

and

$$\int_0^{t_m} \eta(t) \sin \omega_i t dt - A_i \int_0^{t_m} \cos \omega_i t \sin \omega_i t dt - B_i \int_0^{t_m} \sin^2 \omega_i t dt = 0$$

By choosing the length of the record as a multiple of the period $t_m = mT_i$ the integrals over products of sines and cosines vanish and

$$\int_0^{t_m} \cos^2 \omega_i t dt = \int_0^{t_m} \sin^2 \omega_i t dt = \frac{t_m}{2}$$

Hence

$$A_i = \frac{2}{t_m} \int_0^{t_m} \eta(t) \cos \omega_i t dt$$

$$B_i = \frac{2}{t_m} \int_0^{t_m} \eta(t) \sin \omega_i t dt.$$

With the sampled data set $\{\eta_k\}$ and $M = t_m/\Delta t$ where $M + 1 < k_{\max}$, the integrals reduce to sums

$$A_i = \frac{2}{M} \sum_{k=1}^{k=M+1} \eta_k \cos \left(\frac{2\pi(k-1)\Delta t}{T_i} \right)$$

$$B_i = \frac{2}{M} \sum_{k=1}^{k=M+1} \eta_k \sin \left(\frac{2\pi(k-1)\Delta t}{T_i} \right)$$

Hence we can determine the amplitude H_i and phase κ_i of the harmonic component.

$$H_i = \sqrt{A_i^2 + B_i^2}, \quad \tan \kappa_i = \frac{A_i}{B_i}$$

The theory given here can easily be extended to incorporate more components. In case of two dominant components with nearly the same period, as for example M_2 and S_2 the record must be long enough to contain at least one spring neap cycle.

The same method as outlined above applies also when the recorded signal is a current component and the same formulas can be used provided η_k is replaced by u_k , the sampled time series for the current component.

In order to demonstrate the usefulness of the simplified approach we have estimated the amplitudes of M_2 and S_2 for Longyearbyen from a record of sea level from January 1993 with sampling $\Delta t = 1$ hour. For M_2 where $T = 12.42$ hours we use $m = 50$ and $M = 621$ which leads to $H = 53.1$ cm and for S_2 where $T = 12.00$ hours we use $m = 60$ and $M = 720$ which leads to $H = 19.4$ cm. Both amplitudes are in good agreement with the corresponding values in table 2 which are calculated by more accurate methods (Foreman 1977, Pawlowicz et al. 2002).

7 Laplace's tidal equation

The wave length, λ , of the tidal wave is typical of the order 1000 km i.e. much larger than the water depth. Hence a long wave approximation applies with a hydrostatic pressure distribution in the vertical water column:

$$p = p_o + \rho g(\eta - z) \tag{14}$$

Here p_o is the atmospheric pressure, ρ is the mean density of sea water, η is the vertical displacement of the sea surface and z -axis pointing upward with $z = 0$ at the mean sea level. Hence the horizontal pressure gradient becomes

$$\nabla p = \rho g \nabla \eta$$

which shows that the horizontal current associated with the wave motion is essentially depth independent. We denote the horizontal current vector by

$$\vec{v} = \{v_\theta, v_\varphi\}$$

with components directed along the local colatitude (south) and the local longitude (east) respectively. Since the period of the wave motion is of the order of the period of the earth rotation the horizontal components of the Coriolis force, which can be written

$$-f\vec{k} \times \vec{v}$$

will be important. Here $f = 2\Omega \cos \theta$ is the Coriolis parameter with Ω the angular velocity of the Earth and θ the colatitude. \vec{k} is a unit vector pointing upward in vertical direction. Except in some coastal areas the tidal currents are small and the amplitude of the tidal wave, i.e. the height of high water, is much less than the water depth. Hence the equation of motion for the horizontal tidal flow can be linearized and written

$$\frac{\partial \vec{v}}{\partial t} + f\vec{k} \times \vec{v} = -g \nabla (\eta + \tilde{\eta}) - \frac{c_D}{h} |\vec{v}| \vec{v} \quad (15)$$

Here the gradient of the equilibrium tide represent the tide generating force. We have also introduce quadratic bottom friction proportional to v^2 and direction opposite to the current vector. The bottom friction coefficient is denoted c_D which typically is of order $c_D = 0.003$. The dependence of the bottom friction term on water depth ensure that bottom friction is more important in shallow water than in deep water. The equation of continuity can be written

$$\frac{\partial \eta}{\partial t} = -\nabla \cdot (\vec{v}h) \quad (16)$$

which simply expresses that net volume flux into a water column lead to a corresponding displacement of sea level. The horizontal gradient operator in eq (15) and the horizontal divergence operator in eq. (16) are expressed in spherical coordinates θ, φ .

$$\nabla \eta = \left\{ \frac{\partial \eta}{r \partial \theta}, \frac{1}{r \sin \theta} \frac{\partial \eta}{\partial \varphi} \right\} \quad (17)$$

$$\nabla \cdot (\vec{v}h) = \frac{1}{r \sin \theta} \left[\frac{\partial v_\varphi h}{\partial \varphi} + \frac{\partial}{\partial \theta} (v_\theta h \sin \theta) \right] \quad (18)$$

The set of equations (15-16) constitutes *Laplace's tidal equations* (LTE) and are essentially the shallow water equations for long wave motion in a thin fluid layer on a spherical globe. The boundary conditions for LTE are vanishing current perpendicular to the coast

$$\vec{v} \cdot \vec{n} = 0 \quad \text{on} \quad \Gamma_c$$

where \vec{n} is unit vector normal to the coastline, Γ_c .

8 Free wave solution to LTE. Kelvin waves.

Assume that the area of interest is so small that the curvature of the Earth can be neglected. We shall consider an ocean basin with uniform depth h bounded by a

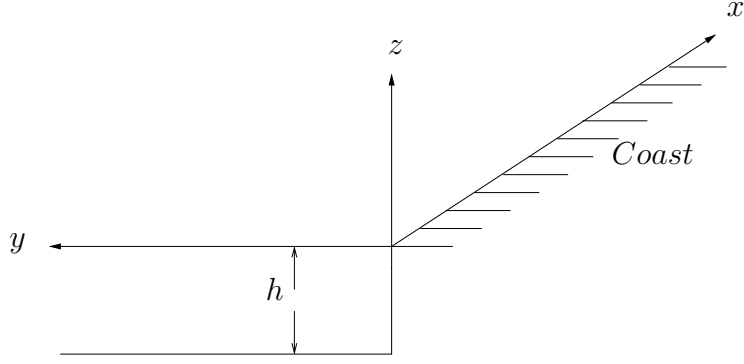


Figure 10: Simple coast geometry for modelling of a Kelvin wave.

straight coast and introduce a Cartesian coordinate system x, y, z as sketched in fig. 10 with the x -axis along the coast and the y -axis in offshore direction.

The components of the horizontal current vector $\vec{v} = \{u, v\}$ and the sea surface displacement η are functions of x, y and time t . Neglecting the bottom friction term and the driving force i.e. the equilibrium tide $\tilde{\eta}$ we obtain from eq. (15)

$$\frac{\partial \vec{v}}{\partial t} + f \vec{k} \times \vec{v} = -g \nabla \eta$$

When written out in component form this equation becomes:

$$\frac{\partial u}{\partial t} - fv = -g \frac{\partial \eta}{\partial x} \quad (19)$$

$$\frac{\partial v}{\partial t} + fu = -g \frac{\partial \eta}{\partial y} \quad (20)$$

Similarly the equation of continuity (16) can be written

$$\frac{\partial \eta}{\partial t} = -h \left(\frac{\partial u}{\partial x} + \frac{\partial v}{\partial y} \right) \quad (21)$$

We will seek a free wave solution propagating in x -direction along the coast

$$\eta = \hat{\eta}(y) \sin k(x - ct)$$

$$u = \hat{u}(y) \sin k(x - ct)$$

$$v = 0$$

where c is the wave speed and k is the wave number. By substitution in eqs. (19-21) we find.

$$\hat{u} = \frac{g}{c} \hat{\eta}$$

$$\frac{d\hat{\eta}}{dy} = -\frac{f}{g} \hat{u}$$

$$\hat{u} = \frac{c}{h} \hat{\eta}$$

Combination of the first and the third of these equations leads to

$$c = \sqrt{gh}$$

and from the second and the third

$$\frac{d\hat{\eta}}{dy} = -\frac{f}{c}\hat{\eta}$$

which can be integrated

$$\hat{\eta} = \eta_0 \exp\left(-\frac{f}{c}y\right)$$

where η_0 is the amplitude at the coast $y = 0$. This shows that the wave propagate with the speed of long waves in shallow water and the amplitude decays exponentially away from the coast. The full solution can now readily be formulated

$$\eta(x, y, t) = \eta_0 \exp\left(-\frac{f}{c}y\right) \sin k(x - ct)$$

$$u(x, y, t) = \frac{c\eta_0}{h} \exp\left(-\frac{f}{c}y\right) \sin k(x - ct)$$

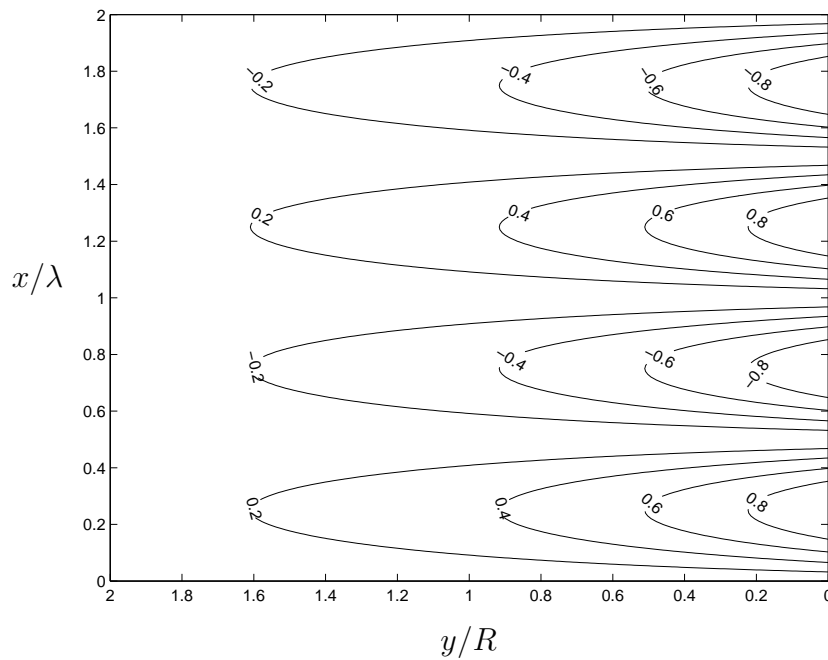


Figure 11: Contour lines for sea level displacement for a Kelvin wave. Normalized to unity at the coast $y = 0$.

Table 4 Parameters for a tidal Kelvin wave.

Amplitude	η_0	1 m
Depth	h	250 m
Wave speed	$c = \sqrt{gh}$	50 m/s
Current	$u_0 = \frac{\eta_0 g}{c}$	0.2 m/s
Period	T	12 hours
Wave length	$\lambda = cT$	2160 km
Coriolis parameter	f	$1.4 \cdot 10^{-4} \text{ s}^{-1}$
Rossby radius	R	357 km

This is known as the *Kelvin wave* solution. The length scale for the damping of the amplitude away from the coast, $R = \frac{c}{f}$, is called the Rossby radius. The numerical example in Table 4 serves to illustrate the properties of a Kelvin wave with 12 hour period. Contour plots of the sea level displacement associated with the Kelvin wave is displayed in fig. 11.

Tidal waves resembles the Kelvin wave in this examples, but in real ocean basins the structure of the waves is modified by bottom topography and bottom friction.

9 Numerical models

Under special conditions with idealized bathymetry and coastline configurations it can easily be shown that the LTE, possess analytical solutions corresponding to *Kelvin waves*, *Sverdrup waves* and topographic Rossby waves (shelf waves). An example to this was given in the previous section. Solutions for realistic bathymetry on global and basin scales are, however, only possible to obtained with numerical methods. Over the last 30 years there have been a large and sustained effort to map the tides in the worlds ocean and in coastal waters by numerical methods (Davies et al. 1996)

In this approach the ocean is divided in grid boxes, most often with a rectangular grid lattice where the values of surface elevation (η) and current (\vec{v}) are specified at the nodes of the lattice. In this description the coastline will appear as piecewise straight lines.

For each grid box the momentum equation (eq. 15) and the continuity equation (eq. 16) are formulated as difference equations where the values of η and (\vec{v}) at the nodes of the lattice are the unknown. With specified boundary condition this set of equations is solved by a computer. Examples of numerical simulations of the tides in the Barents Sea are presented in the next section.

10 Tidal charts for the Barents Sea

In order to describe the structure of the tides in a real ocean we shall, as an example, consider the dynamics of the tides in the Barents Sea and in the regions around Svalbard. The tides in this areas have been simulated by different numerical models which cover the Norwegian, Greenland, Barents Seas and the Arctic Ocean (Gjevik and

Straume 1989, Gjevik et al. 1990, 1994, Kowalik and Proshutinsky 1995 and Lyard 1997). The numerical simulations are based on numerical solutions of Laplace tidal equations with prescribed input along the boundary towards the North Atlantic and the tide generating force on the water masses within the model domain included. It has been shown (Gjevik and Straume 1989) that the inflow by tidal waves from the North Atlantic is the most important factor for the semi-diurnal tides in the Norwegian and the Barents Seas and that the direct effect of the tide generating force within the basin is of less importance. After harmonic analysis of the simulated time series of sea level the results are displayed by contour maps for amplitude, H_i , and phase δ_i for the various harmonic components (figs. 12-15). These type of contour maps are commonly referred to as *tidal charts*. The M_2 chart (fig. 12) display a characteristic circular center with nearly vanishing sea level amplitude south-east of Svalbard. The contour lines for constant phase appear as spokes from the center with increasing phase values when one proceeds in an anticlockwise direction around the center. This type of contour pattern is common in tidal charts and is referred to as an *amphidromic point*. Two other amphidromic points of lesser extent are visible in figure 12. One in the Kara Sea east of Novaja Zemlja and the other one west of Franz Josef Land. The main amphidrome south-east of Svalbard controls the dynamics of the tide in the central parts of the Barents Sea. It shows that a tidal wave is progressing into the Barents Sea with high amplitudes along the coast of Finnmark and with increasing amplitude eastwards along the coasts of Kola. At the same time as the tidal wave crest passes the coast of Finnmark the corresponding crest of the tidal wave is progressing in the deep Norwegian Sea and through the Fram Strait and into the Arctic Ocean north of Svalbard (phase line 030). This wave is propagating around Svalbard and enter the Barents Sea in the straight between Nordaustlandet and Franz Josef Land. This wave leads to a westward propagating wave south of Edge øya and over Svalbardbanken between Svalbard and Bear Island which is evident by the structure of the amphidromic point. The S_2 and N_2 tidal charts (figures 13 and 14) show a similar structure of contour lines as for M_2 implying that these semi-diurnal tidal waves have nearly the same dynamic features as M_2 . The tidal chart for the diurnal component K_1 shows a very different structure particularly with the large amphidromic point in the Fram Strait between Svalbard and Greenland. Also the amphidromic structures south of Svalbard are more complex then for the semi-diurnal components with several local amplitude maxima near the shelf edge. This is a manifestation of that the diurnal tide is resonant with shelf wave modes, with nearly the same period as K_1 , along the pronounced shelf edge between northern Norway and Spitsbergen. The predictions of the model have been validated by comparing with sea level and current measurements. On an average the standard deviation between model and observations is less then 10 % (Gjevik et al. 1994)

An animation of the propagating M_2 tide in the Norwegian and Barents Seas can be found on the internet site: <http://www.farleia-forlag.no>

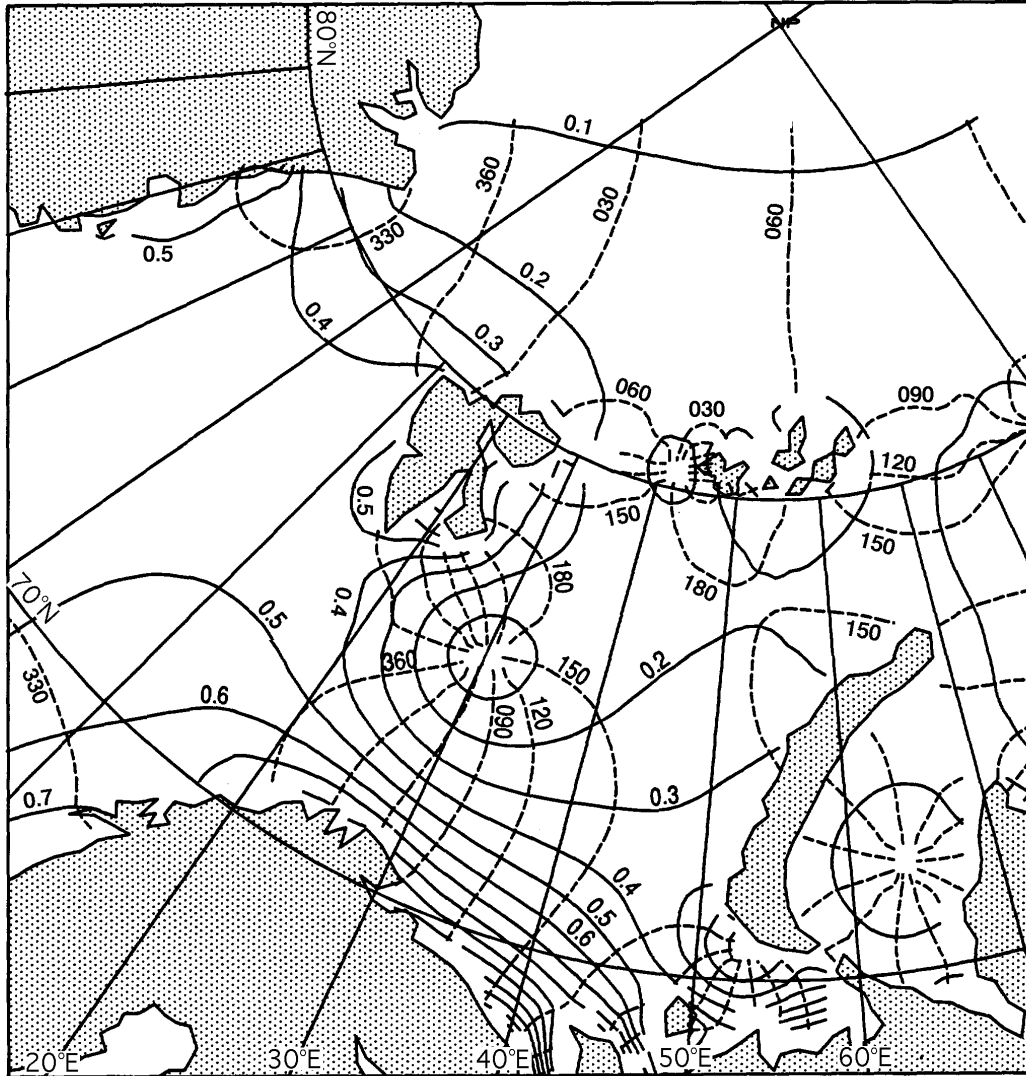
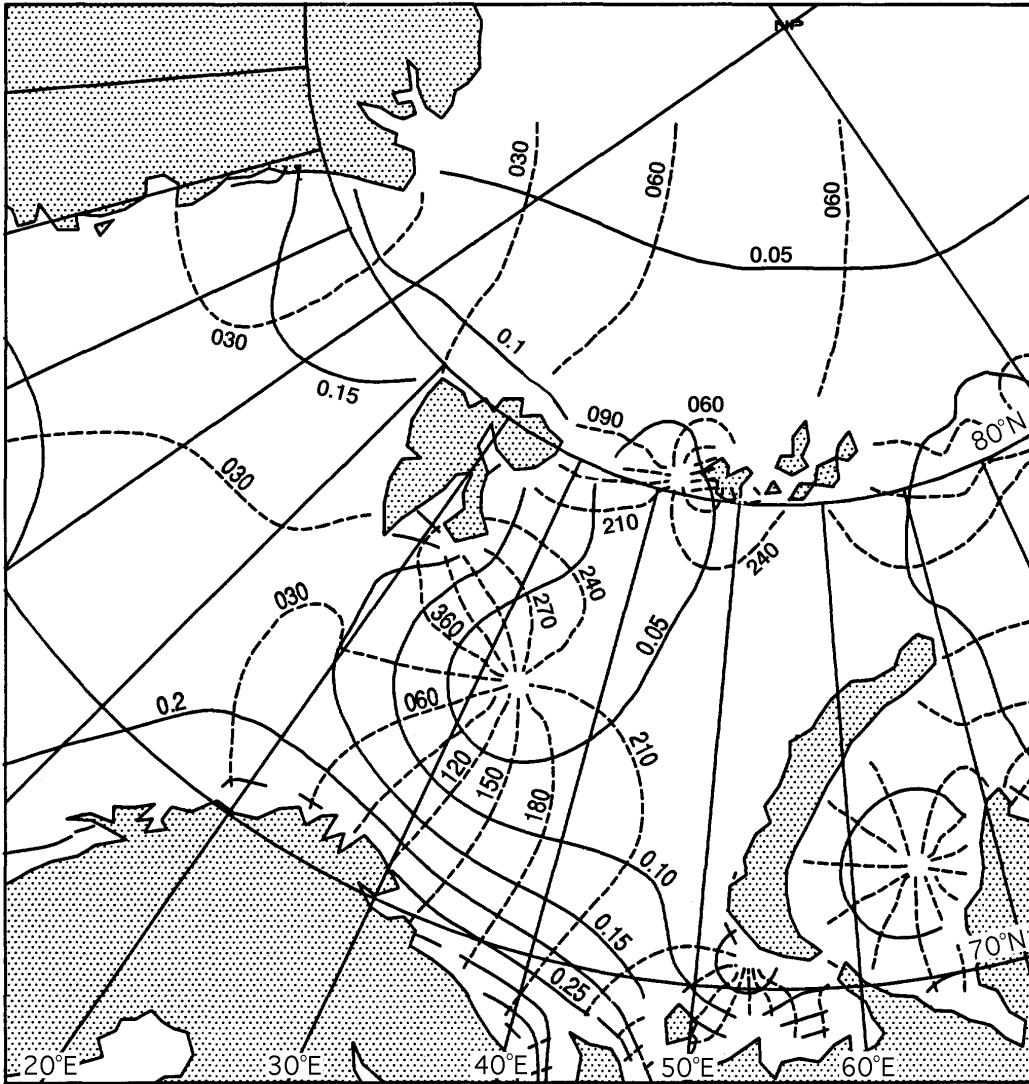


Figure 12: M2 tidal chart. Contour lines for amplitude, H , full drawn lines, phase δ , dotted lines. Units for amplitude meter, for phase degree (Greenwich). From Gjevik, Nøst and Straume, 1994



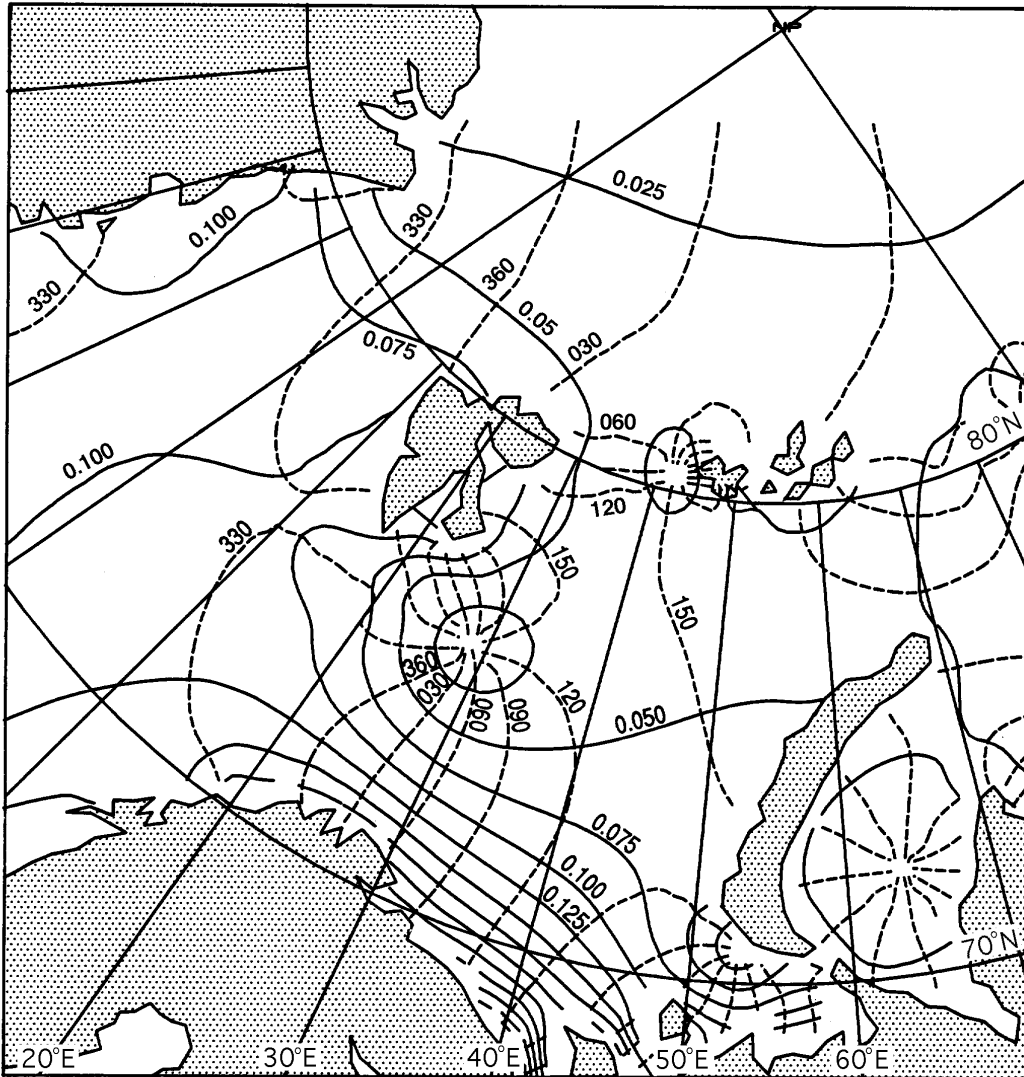


Figure 14: N2 Tidal chart. Contour lines for amplitude, H , full drawn lines, phase δ , dotted lines. Units for amplitude meter, for phase degree (Greenwich). From Gjevik, Nøst and Straume, 1994

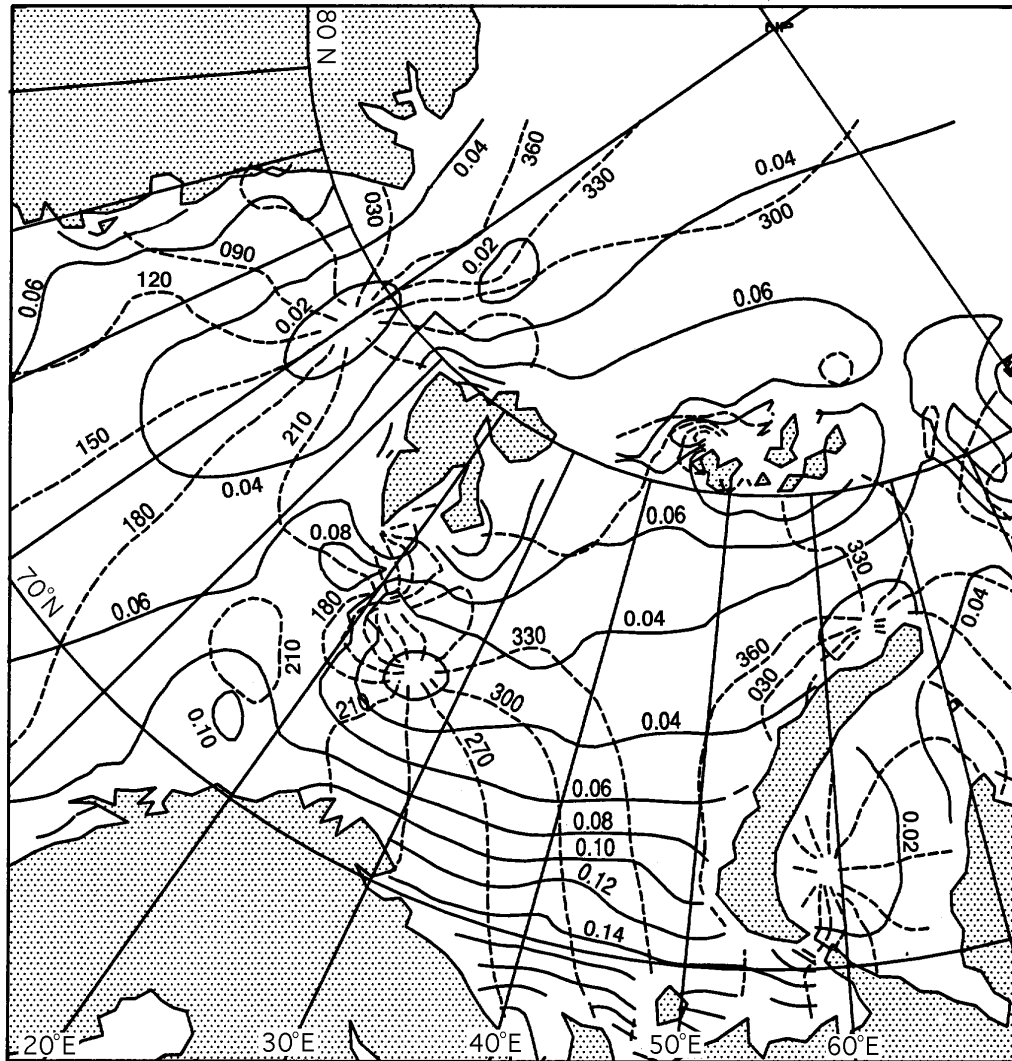


Figure 15: K1 Tidal chart. Contour lines for amplitude, H , full drawn lines, phase δ , dotted lines. Units for amplitude meter, for phase degree (Greenwich). From Gjevik, Nøst and Straume, 1994

11 Tidal currents

Associated with the sea level changes due to tides there are complex current fields. In open deep oceans the tidal current is normally small and of order 1 cm/s. Over shallow banks and in coastal waters where the flow is constrained by topography current speed can be of the order of 1 m/s. In narrow straits and sounds where large water masses pass through during the tidal cycle current speed up to 3-5 m/s may occur. The Maelstrom (Moskstraumen) in Lofoten, northern Norway, is one famous example (Gjevik, Moe and Ommundsen 1997). Strong tidal currents also occur east of Spitsbergen in the Freeman Sound between the Barents Island and Edge Island, in Heleysundet between the Barents Island and Nordaustlandet, and also in the Hinlopen Strait between Spitsbergen and Nordaustlandet (Gjevik 2009).

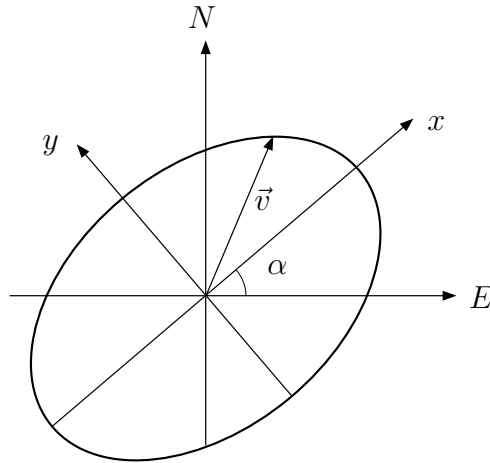


Figure 16: The tidal ellipse

The tidal currents in open sea are generally rotary i.e. the current vector rotates either in a clockwise or a anti-clockwise fashion during the tidal cycle. At the same time the head of the current vector describes an ellipse. With the current vector and its components denoted $\vec{v} = (u, v)$ the *tidal ellipse* can be written

$$\left(\frac{u}{A}\right)^2 + \left(\frac{v}{B}\right)^2 = 1$$

where A and B are the major and minor half axis (A, B) which represent the maximum and minimum current speed respectively. The principal coordinate directions x and y are oriented along the direction of the major and minor half axis of the ellipse which may in general be rotated an angle α relative to local east or north (fig. 16). The current ellipse associated with the M_2 component in the area south of Svalbard is shown in fig 17. Tidal currents are particularly strong over the shallow banks around and northeast of Bear Island. The current ellipses are here nearly circular with a clockwise rotation of the current vector. Maximum current speed is up to 1.0 m/s which is an exceptional large current in open ocean.

Due to the effect of friction and turbulence the tidal current may vary considerably in the vertical. Density stratification may also modify the current profile and lead to

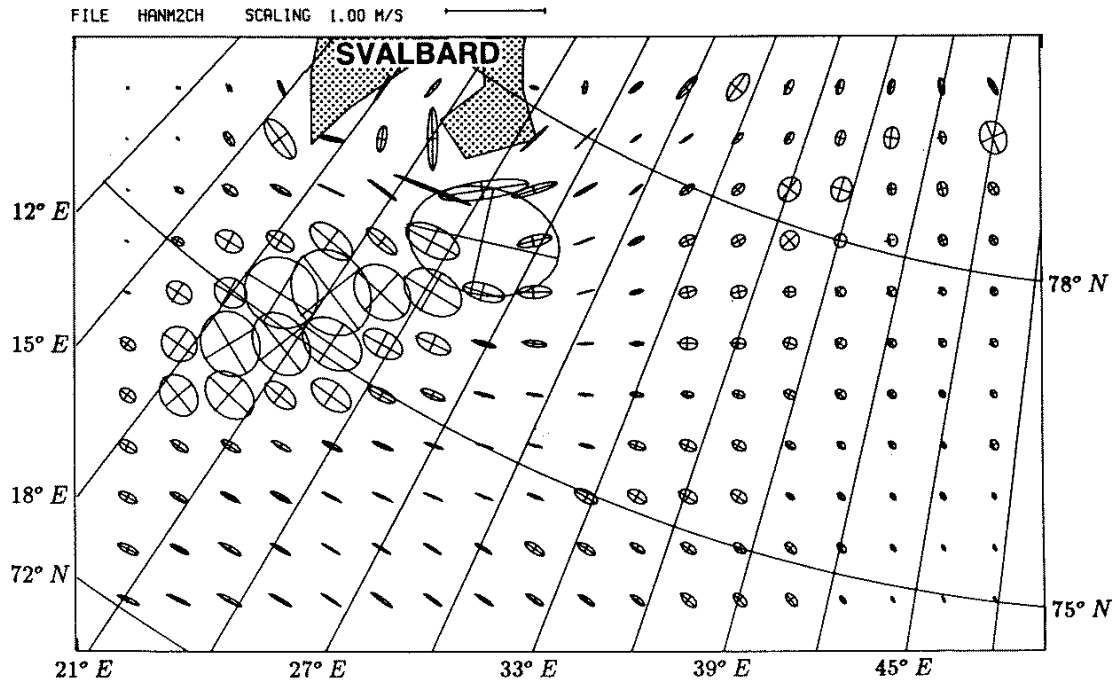


Figure 17: The M_2 tidal ellipses south of Svalbard. From Gjevik et al. 1990

internal wave modes (internal tides). This is particularly important in fjords (Tverberg et al. 1991).

Near the critical latitude where the period of the tide coincides with the inertial period, it can be shown that turbulence and stratification will have a dominant effect on the profile of the tidal current. The critical latitude for the M_2 component is $75^\circ 2.8'$ which passes through the Barents Sea north of Bear Island. Nøst (1994) found that current data from this area show the expected influence on the tidal current profile matching model predictions. Similar results from the area near the southern critical latitude in the Wedell Sea were reported by Foldvik et al. (1990).

12 Drift and dispersion of particles in the tidal flow

In areas with strong tidal currents it represents a major factor for drift and dispersion of particles suspended in the water column. Since particles which are displaced during the first part of the tidal cycle may move into an area with a different current regime, the particles will not necessarily return along the same path during the second part of the tidal cycle. Hence a net displacement or drift may occur. The tide will, for example, lead to a tidal-induced clockwise circulation around Bear Island where particles will circumvent the island in 6-8 days. This has been documented both from observations (Vinje et al. 1989) and by model and laboratory studies (Straume et al. 1994, Gjevik et al. 1994, Kowalik and Proshutinsky 1995, and Gjevik 1996).



Figure 18: Streamlines showing strong tidal current in Ormholet near Heleysundet between Bar-entsøya and Nordaustlandet. (Photo by courtesy of Prof. Johan Ludvig Sollid).

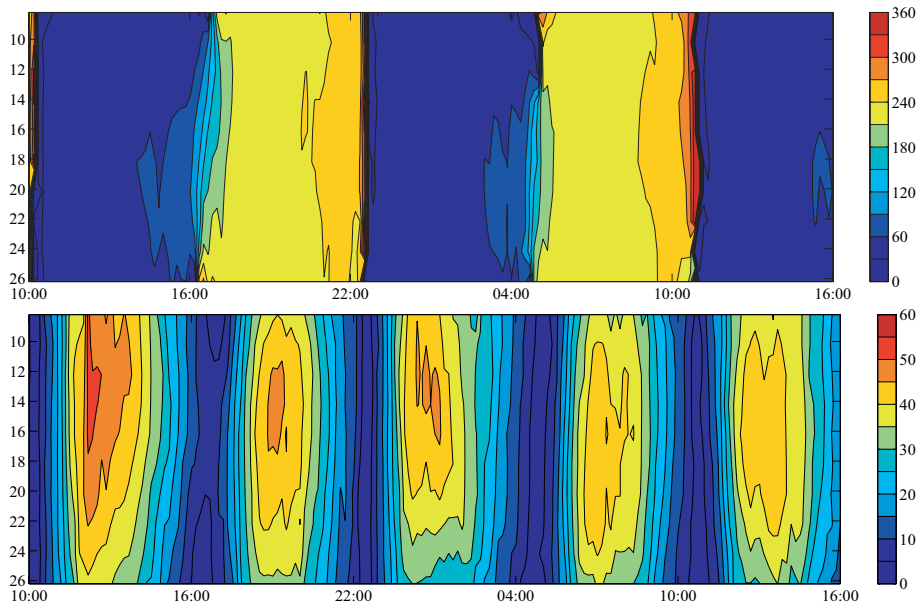


Figure 19: Regular tidal current oscillations under sea ice near Cape Lee in the western part of the Freeman Sound. ADCP records from 10 AM on 19 April to 16 PM on 20 April 2004 (local time). The measurements cover from 9 to 26 meter depth. Upper graph current direction in degree true. Lower graph current speed in cm/s. See color scale on right side. (Smedsrud and Skogseth 2004).

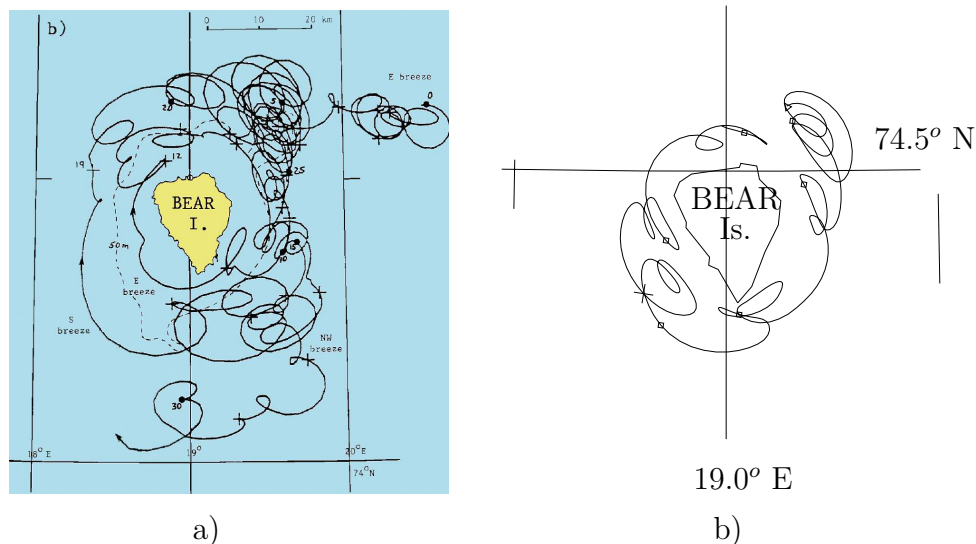


Figure 20: Observed 30 days drift of Argos buoy around Bear Island (a) (After Vinje et al., 1989). Particle trajectories in tidal current from model simulations (7 days) (b). (Straume et al. 1994, Gjevik 1996)

13 Mean sea level (MSL)

Mean sea level serves as a reference height or datum for tidal sea level displacements and also for land surveying. Tidal amplitudes usually refer to MSL and the heights of mountains and hills on maps are given relative to MSL.

Mean sea level can be determined from long records of sea level observations by eq. 12. For averaging out the effect of tidal oscillations in the records MSL is calculated for a period of 19 years which covers the longest period of oscillation of the tide generating force from the Moon (18.6 years). MSL for this long averaging period is regularly updated and used for references. Monthly and annual mean values of MSL are also calculated and published by the national Hydrographic Services all over the world.

Observed variation in annual mean sea level can provide information on land upheaval or subsidence and climate changes. For example; data from Oslo, Norway (fig. 21) show a gradual lowering of mean sea level of about 30 cm over a period of 85 years, corresponding to land rise of about 0.39 cm/year. This is due to the still ongoing rebound of the Earth crust after it was suppressed by the ice load during the Pleistocene ice age.

Data from stations along the western and northern coast of Norway (fig. 22) show coherent decadal variations in mean sea level. In the years 1982-83 and 1988-91 sea level was higher than usual and this correlates to positive values of the NAO index (fig. 23). It is not unexpected that the oscillations in The North Atlantic weather system, as expressed by the NAO index, manifest itself by variation in mean sea level along the Norwegian coast. The explanation is of course that the strengthening of the westerly wind stress over The North Atlantic and The Norwegian Sea, in period with large positive NAO index, leads to a transport of water towards the Norwegian coast and thereby an increase in sea level. Analysis of MSL data have become an important

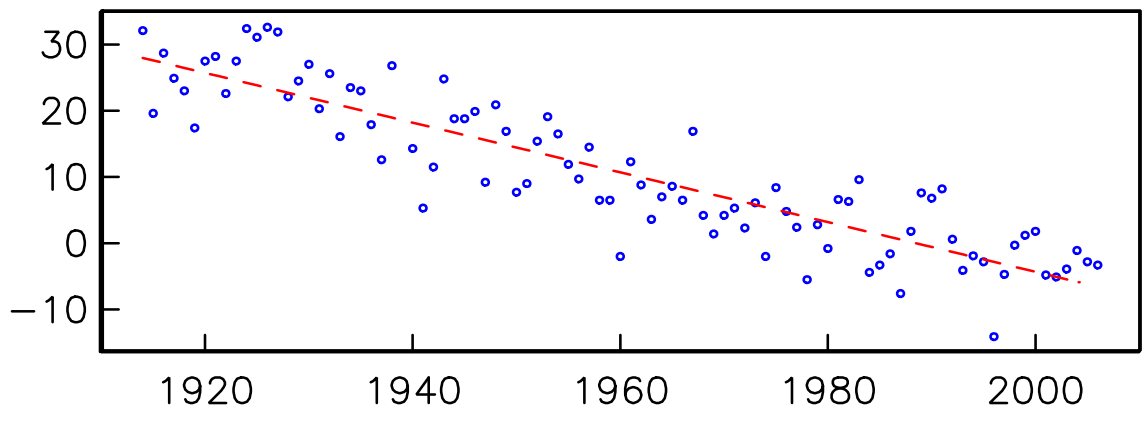


Figure 21: Annual mean sea level (in centimeter) at Oslo for the years 1914-2006 (blue rings). Broken red line is best regression fit corresponding to a lowering of mean sea level of 0.38 cm/year. From Gjevik (2009).

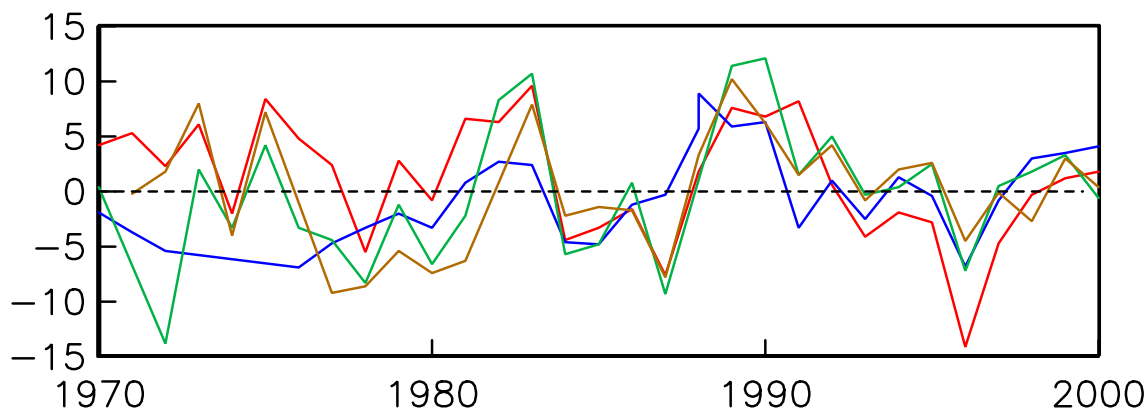


Figure 22: Variation in annual mean sea level (in centimeters) at four stations along the Norwegian coast in the years 1970-1999, Oslo (red), Bergen (blue), Bodø (green) and Hammerfest (brown). From Gjevik (2009).

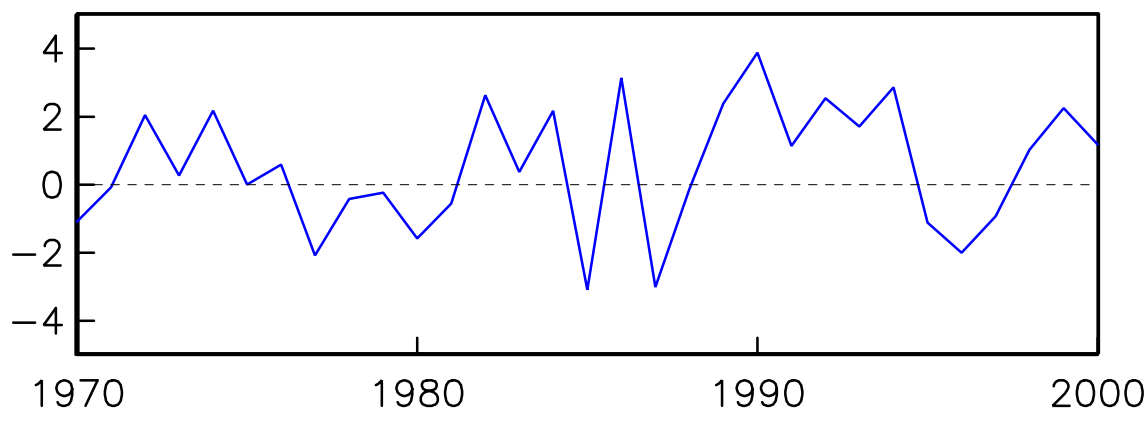


Figure 23: Difference in atmospheric pressure at sea level between Ponta Delgada at The Azores and Stykkisholmur near Reykjavik on Iceland. Here expressed by the NAO-index (annual mean) for the years 1970-1999. Positive value of the NAO index corresponds to highest air pressure at The Azores. (From Jim Hurrell, NCAR)

tool for climate studies and climate modelling.

An international data archive, named the Permanent Service for Mean Sea Level (PSMSL), has therefore been established at Proudman Oceanographic Laboratory, England and MSL data from a world wide network of stations can be down loaded from its data base (www.pol.ac.uk/psmsl).

14 Exercises

1. Calculate the phase angle difference corresponding to a time delay of one hour for each of the tidal components listed in table 2.
2. Find the time delay between the Moon's transit over the Greenwich meridian and the next high water in Longyearbyen. Consider mean high water as given by the M_2 component. What will be the time delay relative to the Moon's transit over the local meridian through Longyearbyen?
3. At a location with predominate semi-diurnal tide the amplitude at spring is 75 cm and at neap 35 cm. What are approximately the amplitude of the M_2 and S_2 components?
4. Assume that the tide is adequately described by only two tidal components M_2 and S_2 . What is the exact time between neap and spring tide in this case ?
5. The minimum and maximum distance between the centers of the Moon and the Earth is about 356.500 km and 406.700 km respectively. Calculate the peak tidal acceleration in perigee and apogee position in percentage of the mean value.
6. What is approximately the time period between events with the perigee at the time of full Moon?
7. Use the tidal tables (ref. [24]) or tidal predictions available on the internet site vannstand.no to find time for high and low water (LW and HW) on 27 September 2013 at Kirkenes and Longyearbyen. Show that the time difference for HW and LW between these two stations correspond approximately to the phase angle difference for the M_2 component.
8. Assume that sea level is responding to changes in atmospheric pressure in a quasi steady barometric fashion such that the weight of the access water column corresponds directly to the change in atmospheric pressure. How large changes in the atmospheric pressure (in hPa) are required to explain the difference between predicted and observed sea level in fig. 9 ?
9. On basis of the tidal charts for the Barents Sea try to explain that large tidal currents are to be expected in the Freeman Sound between the Barents Island and Edge Island east of Spitsbergen.
10. Use the phase information for M_2 in the chart fig. 12 to estimate the average speed of the tidal wave along the coast of Finnmark and Kola. With the formula \sqrt{gh} for the speed of long water waves find the corresponding depth. Check the depth on maps of the area to see if this is a reasonable estimate.

11. The tidal current is given by its velocity components $u = u_o \sin \omega t$, $v = v_o \cos \omega t$ in a Cartesian coordinate system x, y . u_o, v_o are constants ω is the angular velocity and t is time. Consider a particle which at $t = 0$ is located at the origin and subsequently drifts passively with the current. Find the path or the trajectory for the particle. What is the maximum displacement (tidal excursion) of the particle in the x and y direction respectively?
12. Suppose that we add a mean current \bar{u} along the x -axis to the tidal oscillations in problem 11. Determine the path of a particle released at the origin at $t = 0$ and sketch the trajectory when $\bar{u} = \frac{u_o}{2}$ and $\bar{u} = 2u_o$.

References

- [1] Cartwright, E. D., (1977) Oceanic tides. *Rep. Prog. Phys.* **40**, 665-708.
- [2] Davies, M. A., J. E. Jones and J. Xing, (1996) A review of recent development in tidal hydrodynamic modelling, parts I and II. *J. Hydraulic Eng. ASCE*, **123**, No 4, 278-302.
- [3] Foldvik, A., J. H. Middleton and T. D. Foster (1990) Tides in the southern Wedell Sea. *Deep Sea Res.*, **37**, 1345-1362.
- [4] Foreman, M. G. G., (1977) Manual for tidal heights analysis and predictions. *Pac. Mar. Sci. Rep.*, **77-10**, 101 pp. Inst. Ocean Sci. Sidney, B.C. Canada.
- [5] Gjevik, B., and T. Straume, (1989), Model simulation of the M_2 and the K_1 tide in the Nordic Seas and the Arctic ocean. *Tellus* **41A**, pp. 73-96.
- [6] Gjevik, B., (1990) Model simulations of tides and shelf waves along the shelves of the Norwegian-Greenland-Barents Seas. *In: Modelling Marine Systems Ed. A.M. Davies, CRC Press Inc. Vol. I*, pp. 187-219.
- [7] Gjevik, B., E. Nøst, and T. Straume, (1990), Atlas of tides on the shelves of the Norwegian and the Barents Seas. *Dept. of Math., Univ. of Oslo, report FoU-ST 90012 to Statoil, Stavanger*.
- [8] Gjevik, B., E. Nøst and T. Straume, (1994), Model simulations of the tides in the Barents Sea. *J. Geophysical Res.*, **Vol 99**, No C2, 3337-3350.
- [9] Gjevik, B., (1996) Models of drift and dispersion in tidal flows. In *Waves and Non-linear Processes in Hydrodynamics*. Eds. J. Grue, B. Gjevik and J. E. Weber. Kluwer Academic Publisher, pp. 343-354.
- [10] Gjevik, B., H. Moe og A. Ommundsen, (1997), Sources of the Maelstrom. *Nature*, **Vol 388**, 28 August 1997, 837-838.
- [11] Gjevik, B., (2009) Flo og fjære langs kysten av Norge og Svalbard. Farleia Forlag. ISBN 978-82-998031-0-6.
- [12] Kowalik, Z. and A. Yu. Proshutinsky, (1995), Topographic enhancement of tidal motion in the western Barents Sea. *J. Geophys. Res.*, **Vol. 100, no. C2**, 2613-2637.

- [13] Laplace P. S. (1775) Recherches sur Quelques Points de Systeme du Monde. *Mem. Acad. Roy. Sci.* **88**.
- [14] Lyard, F. H., (1997) The tides in the Arctic Ocean from a finite element model. *J. Geophys. Res.*, **Vol. 102, no. C7**, 15611-15638.
- [15] Newton I. (1687) *Philosophiae Naturalis Principia Mathematica*, London.
- [16] Nøst, E., (1994) Calculating tidal current profiles from vertically integrated models near the critical latitude in the Barents Sea *J. Geophys. Res.*, **Vol. 99, no. C4**, 7885-7901.
- [17] Pawlowicz, P., Beardsley, B., and Lentz, S. (2002) Classical tidal analysis including error estimated in Matlab using T-tide. *Computers and Geoscience* **28**, 929-937.
- [18] Schwiderski, E. W., (1980) On charting global ocean tides. *Rev. Geophys. and Space Physics* **18**, 243-268.
- [19] Schwiderski, E. W., (1986) Tides. *In The Nordic Seas (ed. B. G. Hurdle): New York Springer-Verlag, 191-209.*
- [20] Lars H. Smedsrud and Ragnheid Skogseth (2006) Field measurements of Arctic grease ice properties and processes. *Cold Regions Science and Technology*, Vol. 44, 171-183.
- [21] Sato, T. et al. (2006) A geophysical interpretation of the secular displacement and gravity rates observed at Ny-Alesund, Svalbard in the Arctic– effects of post-glacial rebound and present-day ice melting. *Geophysical Journal International* **Vol. 165**, 729–743.
- [22] Straume. T., J. H. Nilsen, T. A. McClimans, and B. Gjevik, (1994), Circulation around Bear Island in the Barents Sea: Numerical and laboratory simulations. *Annales Geophysicae, Vol. 12 suppl. II, C 277, Abstract to EGS-General Assembly, Grenoble.*
- [23] Thomson, W. (lord Kelvin) (1868) Report of Committee for the Purpose of Harmonic Analysis of Tidal Observations. *British Association for the Advancement of Science, London.*
- [24] Tidevannstabeller for den norske kyst med Svalbard (2013), *Statens Kartverk, Sjøkartverket, Stavanger.*
- [25] Tverberg, V., H. Cushman-Roisin and H. Svendsen, (1991) Modeling internal tides in fjords *J. Marine Res.* **49**, 635-658.
- [26] Vinje. T., H. Jensen, A. S. Johnsen, S. Løset, S. E. Hamran, S. M. Løvas, and B. Erlingsson, (1989), IDAP-89 R/V Lance deployment. Vol. 2; Field observations and analysis. *Norwegian Polar Research Institute, Oslo and SINTEF/NHL, Trondheim 80pp.*